Pergamon

Engineering Fracture Mechanics Vol. 54, No. 5, pp. 703–711, 1996

0013-7944/96 $15.00 + 0.00

0013-7944(95)00203-0

FRACTAL TWO-LEVEL FINITE ELEMENT METHOD FOR CRACKED KIRCHHOFF'S PLATES USING DKT ELEMENTS

A. Y. T. LEUNG and R. K. L. SU

Department of Civil and Structural Engineering, University of Hong Kong, Pokfulam Road, Hong Kong

Abstract—A technique for calculating moment intensity factors (MIF) and stress intensity factors (SIF) for through-thickness cracks in thin plates subjected to out-of-plane bending by means of fractal two-level finite element method is proposed. It is based on the nodal displacements transformation near the crack tip in terms of some analytical functions. The similarity characteristic properties of the plate element stiffness are employed. Fractal transformation technique is developed to transform infinitely many nodal displacements around the crack tip to a small set of generalized displacements including the MIF and SIF as direct unknowns. Examples are given on the centre cracked plates in bending. The results are in good agreement with analytical results and with other researchers. Comparison of the results from Kirchhoff's theory and from Reissner's plate theory shows large differences up to *ca* 50%. Copyright © 1996 Elsevier Science Ltd

INTRODUCTION

IN ENGINEERING applications of the principles of linear elastic fracture mechanics to through cracked plates subject to out-of-plane bending, expressions for the moment intensity factors and shear intensity factors [1] must be determined. Knowles and Wang [2] discovered the differences in the predictions of stress intensity factors between Kirchhoff's and Reissner's theories. He considered an infinite plate with crack of length $2a$, subjected to remote all round bending moment M_0, Reissner's shear deformation theory leads to $K_1 = (1 + \nu)/(3 + \nu)M_0\sqrt{a}$ instead of $K_1 = M_0\sqrt{a}$ from Kirchhoff's theory [1]. The thickness effects of infinite Reissner's plate were studied by Hartranft and Sih [3], and Wang [4]. Hartranft reported that the moment intensity factor increases 62% when the plate thickness increases from zero to approximately one-tenth of the crack length for $\nu = 0.3$. However, bending of finite cracked plates is probably of more practical significance than that of infinite plate. The moment intensity factor of finite cracked plate was deliberated by Wilson and Thompson [5] using Kirchhoff's theory and finite element method. About one decade later, Murthy *et al.* [6] applied shear deformation theory to solve cracked finite plate analytically, later Boduroglu and Erdogan [7] used singular integral equations, and most recently Leung and Su [8] employed numerical method to solve the similar problems.

It is our intention to extend the fractal two-level finite element method (F2LFEM) [9, 10] to solve the solution of "thin" crack plate subjected to bending. While the interpolating shape functions within a finite element reduce a continuum of an infinite number of degrees of freedom to a finite number of degrees of freedom in terms of the nodal displacements, global interpolating functions for the nodal displacements can also be used to drastically reduce the number of unknowns. The global interpolating functions can be obtained by eigenfunction expansion technique based on Kirchhoff's plate theory. Fractal transformation method is introduced so that an infinite number of finite elements with infinitely many degrees of freedom can be transformed in an expeditious way.

To fix ideas, suppose that a plate with a crack is discretized into conventional finite elements. The nearer to the crack tip, the finer will be the mesh. Analytical solutions are available in the region very near to the singular point. Therefore, the nodal displacements of the fine mesh near the crack tip follow certain known analytical patterns. It is reasonable to interpolate the nodal displacements by the known solutions. The unknowns at the singular region are no longer the nodal displacement, but the coefficient of the global interpolating functions of the nodal displacement. Since the analytical solutions are valid only in the vicinity of the crack tip, outside the singular region, the solutions are obtained by the conventional finite elements methods. The advantage of

being capable to model complex boundary conditions is preserved. The stiffness matrix associated with the coefficients is obtained by matrix transformation. In fact, the transformation is performed at element level so that the order involved is very small. The crack parameters, stress intensity factors or moment intensity factors can be obtained directly from the coefficients.

GLOBAL INTERPOLATING FUNCTION

By using Kirchhoff's theory for plates in bending, the appropriate differential equation controlling the deflection $w(r,\theta)$ is

$$\nabla^4 w(r,\theta) = q(r,\theta)/D\ , \tag{1}$$

in which D (the flexible rigidity) is given by $D = Eh^3/12(1-\nu^2)$; E is Young's modulus and ν is Poisson's ratio. The moments M_r, M_θ and $M_{r\theta}$ and shears Q_r and Q_θ can be related with the deflection w as follows

$$M_r(r,\theta) = -D\left[\frac{\partial^2 w}{\partial r^2} + \nu\left(\frac{1}{r}\frac{\partial w}{\partial r} + \frac{1}{r^2}\frac{\partial^2 w}{\partial \theta^2}\right)\right]$$

$$M_\theta(r,\theta) = -D\left[\frac{1}{r}\frac{\partial w}{\partial r} + \frac{1}{r^2}\frac{\partial^2 w}{\partial \theta^2} + \nu\frac{\partial^2 w}{\partial r^2}\right]$$

$$M_{r\theta}(r,\theta) = (1-\nu)D\left[\frac{1}{r}\frac{\partial}{\partial \theta}\left(\frac{\partial}{\partial r} - \frac{1}{r}\right)\right]w$$

$$Q_r(r,\theta) = -D\left[\frac{\partial}{\partial r}(\nabla^2 w) + \frac{1}{r}\frac{\partial}{\partial \theta}(M_{r\theta})\right]$$

$$Q_\theta(r,\theta) = -D\left[\frac{1}{r}\frac{\partial}{\partial \theta}(\nabla^2 \theta) + \frac{\partial}{\partial r}(M_{r\theta})\right]. \tag{2}$$

Assuming the traction-free boundary conditions at the crack faces, one has the boundary conditions

$$M_\theta = M_{r\theta} = Q_\theta = 0 \text{ for } \theta = \pm\pi\ . \tag{3}$$

It has been shown by Williams [11] that the desired characteristic solutions are of the form

$$(1-\nu)Dw_n(r,\theta) = r^{(n+2)/2}[b_1\cos(n/2+1)\theta + b_2\sin(n/2+1)\theta + b_3\cos(n/2-1)\theta + b_4\sin(n/2-1)\theta]$$
$$(\text{for } n = 1,2,\ldots)$$

and for the rigid body motion,

$$w_0(r,\theta) = b_1 r\cos(\theta) + b_2 r\sin(\theta) + a_0\ , \tag{4}$$

where a_0 and b_i ($i = 1$–4) are the arbitrary constants. The relations between the constants are found by replacing eq. (4) into eq. (3) to yield

$$b_3 = b_1\frac{(n+2)(1-\nu)}{(-n+(-1)^n 6)+(n+(-1)^n 2)\nu} \text{ and } b_4 = b_2\frac{(n+2)(1-\nu)}{(-n-(-1)^n 6)+(n-(-1)^n 2)\nu}\ . \tag{5}$$

By neglecting the shear deformation, the rotational displacements are

$$\psi_r = \frac{\partial w}{\partial r} \text{ and } \psi_\theta = \frac{1}{r}\frac{\partial w}{\partial \theta}\ . \tag{6}$$

Letting $b_1 = B_n^{(1)}$ and $b_2 = B_n^{(2)}$, substituting eq. (5) into eq. (4a) and then into eq. (6), the displacement distribution in the vicinity of the end of a crack is expressed in the form:

$$(1-v)D\psi_{m} = \frac{r^{n/2}}{2} B_n^{(1)}\left[(n+2)\cos(n/2+1)\theta + \frac{(n+2)^2(1-v)}{(-n+(-1)^n 6)+(n+(-1)^n 2)v}\cos(n/2-1)\theta\right]$$

$$+ \frac{r^{n/2}}{2} B_n^{(2)}\left[(n+2)\sin(n/2+1)\theta + \frac{(n+2)^2(1-v)}{(-n-(-1)^n 6)+(n-(-1)^n 2)v}\sin(n/2-1)\theta\right]$$

$$(1-v)D\psi_{0n} = -\frac{r^{n/2}}{2} B_n^{(1)}\left[(n+2)\sin(n/2+1)\theta + \frac{(n^2-4)(1-v)}{(-n+(-1)^n 6)+(n+(-1)^n 2)v}\sin(n/2-1)\theta\right]$$

$$+ \frac{r^{n/2}}{2} B_n^{(2)}\left[(n+2)\cos(n/2+1)\theta + \frac{(n^2-4)(1-v)}{(-n-(-1)^n 6)+(n-(-1)^n 2)v}\cos(n/2-1)\theta\right]$$

$$(1-v)Dw_n = r^{(n+2)/2} B_n^{(1)}\left[\cos(n/2+1)\theta + \frac{(n+2)(1-v)}{(-n+(-1)^n 6)+(n+(-1)^n 2)v}\cos(n/2-1)\theta\right]$$

$$+ r^{(n+2)/2} B_n^{(2)}\left[\sin(n/2+1)\theta + \frac{(n+2)(1-v)}{(-n(-1)^n 6)+(n-(-1)^n 2)v}\sin(n/2-1)\theta\right]. \quad (7)$$

Furthermore, the displacement distribution (ψ_1, ψ_2, w) in the rectangular coordinates system as shown in Fig. 1 is given by the transformation,

$$\begin{Bmatrix}\psi_1\\ \psi_2\\ w\end{Bmatrix} = \begin{bmatrix}\cos(\theta) & -\sin(\theta) & 0\\ \sin(\theta) & \cos(\theta) & 0\\ 0 & 0 & 1\end{bmatrix}\begin{Bmatrix}\psi_r\\ \psi_\theta\\ w\end{Bmatrix}. \quad (8)$$

With the aids of eqs (7) and (8), the general displacement distribution in the vicinity of a crack tip can be derived. It will be used as the global interpolation function.

The moment intensity factors K_1 and K_2 are defined as follows,

$$K_1 = \lim_{r\to 0}\sqrt{2rM_{22}(r,0)}$$

$$K_2 = \lim_{r\to 0}\sqrt{2rM_{12}(r,0)}\,. \quad (9)$$

They can be obtained by substituting eq. (7) into eq. (2) and putting $\theta = 0$,

$$K_1 = \frac{3\sqrt{2}(3+v)}{(7+v)} B_1^{(1)} \text{ and } K_2 = \frac{3\sqrt{2}(1+v)}{(5+3v)} B_1^{(2)}\,. \quad (10)$$

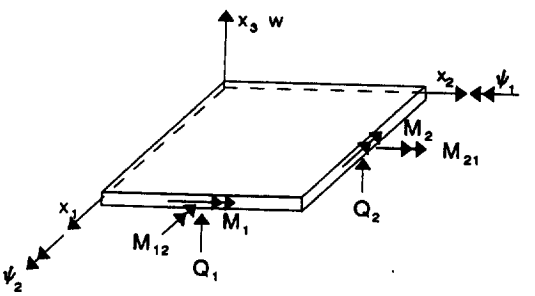

Fig. 1. Notations for Kirchhoff's plate.

Explicit dependence of the stress intensity factors $k_1(x_3)$ and $k_2(x_3)$ with the transverse coordinate x_3 is obtained by means of the relations,

$$k_1(x_3) = \frac{12x_3}{h^3} K_1 \text{ and } k_2(x_3) = \frac{12x_3}{h^3} K_2 . \tag{11}$$

The evaluation of moment intensity factors or stress intensity factors are reduced to the determination of the coefficients $B_1^{(1)}$ and $B_1^{(2)}$.

STIFFNESS MATRICES OF PLATE BENDING ELEMENTS WITH SIMILAR SHAPE

In this section the property of the selected plate bending elements with similar shape will be explored. A triangular nine degree-of-freedom element, namely a discrete Kirchhoff theory (DKT) element [12], is chosen for the subsequent finite element analysis because of the efficiency and reliability of the element [13].

Consider a triangular DKT element with thickness h and with the area of the middle surface of the plate A, the stiffness matrix of the DKT element can be expressed as

$$\boldsymbol{K} = \int_A \kappa' \boldsymbol{D} \kappa \mathrm{d}x\mathrm{d}y , \tag{12}$$

where the material matrix $\boldsymbol{D}$ and the strain–displacement matrix κ are given as

$$\boldsymbol{D} = \frac{Eh^3}{12(1-\nu^2)} \begin{bmatrix} 1 & \nu & 0 \\ \nu & 1 & 0 \\ 0 & 0 & \dfrac{1-\nu}{2} \end{bmatrix} \tag{13}$$

and

$$\kappa = \begin{Bmatrix} \dfrac{\partial \alpha}{\partial x} \\ \dfrac{\partial \beta}{\partial y} \\ \dfrac{\partial \alpha}{\partial y} + \dfrac{\partial \beta}{\partial x} \end{Bmatrix} . \tag{14}$$

Here, α and β are the rotations of the normal to the undeformed middle surface in the x_1–x_3 and x_2–x_3 planes, respectively, and they are related to the element degrees of freedom as

$$\alpha = \langle \bar{G} \rangle \{\delta\} \text{ and } \beta = \langle \bar{H} \rangle \{\delta\} , \tag{15}$$

where $\{\delta\}' = \{\psi_{11}\ \psi_{21}\ w_1\ \psi_{12}\ \psi_{22}\ w_2\ \psi_{13}\ \psi_{23}\ w_3\}$ is the nodal rotations and deflections vector.

The shape function row vectors $\langle \bar{G} \rangle$ and $\langle \bar{H} \rangle$ are presented explicitly in terms of area coordinates ξ and η, by

$$\langle \bar{G} \rangle = \{1\ \xi\ \eta\ \xi^2\ \xi\eta\ \eta^2\}[G] \text{ and } \langle \bar{H} \rangle = \{1\ \xi\ \eta\ \xi^2\ \xi\eta\ \eta^2\}[H] \tag{16}$$

$$[G]_t = \begin{bmatrix} -1 & 3+4c_6 & 3+4c_5 & -2-4c_6 & -4-4c_5-4c_6 & -2-4c_5 \\ 0 & 4b_6 & 4b_5 & -4b_6 & -4b_5-4b_6 & -4b_5 \\ 0 & 6a_6 & -6a_5 & -6a_6 & 6a_5-6a_6 & 6a_5 \\ 0 & 1+4c_6 & 0 & -2-4c_6 & 4c_4-4c_6 & 0 \\ 0 & 4b_6 & 0 & -4b_6 & 4b_4-4b_6 & 0 \\ 0 & -6a_6 & 0 & 6a_6 & 6a_4-6a_6 & 0 \\ 0 & 0 & 1+4c_5 & 0 & 4c_4-4c_5 & -2-4c_5 \\ 0 & 0 & 4b_5 & 0 & 4b_4-4b_5 & -4b_5 \\ 0 & 0 & 6a_5 & 0 & -6a_4-6a_5 & -6a_5 \end{bmatrix} \tag{17}$$

$$[H]' = \begin{bmatrix} 0 & 4b_6 & 4b_5 & -4b_6 & -4b_5 - 4b_6 & -4b_5 \\ -1 & 3+4e_6 & 3+4e_5 & -2-4e_6 & -4-4e_5-4e_6 & -2-4e_5 \\ 0 & 6d_6 & -6d_5 & -6d_6 & 6d_5 - 6d_6 & 6d_5 \\ 0 & 4b_6 & 0 & -4b_6 & 4b_4 - 4b_6 & 0 \\ 0 & 1+4e_6 & 0 & -2-4e_6 & 4e_4 - 4e_6 & 0 \\ 0 & -6d_6 & 0 & 6d_6 & 6d_4 - 6d_6 & 0 \\ 0 & 0 & 4b_5 & 0 & 4b_4 - 4b_5 & -4b_5 \\ 0 & 0 & 1+4e_5 & 0 & 4e_4 - 4e_5 & -2-4e_5 \\ 0 & 0 & 6d_5 & 0 & -6d_4 - 6d_5 & -6d_5 \end{bmatrix} \tag{18}$$

in which a_k, b_k, c_k, d_k and e_k ($k = 4$–6) are defined in ref. [13].It is noted that the coefficients a_k and d_k are in dimension L^{-1} and the rest of the coefficients are dimensionless.

Two elements, denoted 1 and 2, have a shape which is similar with the length ratio λ. The relationships of the coordinates for the corresponding nodes can be represented by

$$x_{1i}^2 = \lambda x_{1i}^1 \text{ and } x_{2i}^2 = \lambda x_{2i}^1, \tag{19}$$

where x_{ji}^k are the coordinates of element k at node i.

Without loss of generality, the element stiffness matrix for element 1 is partition according to $\{\psi^1\}' = \{\psi_{11}^1\psi_{12}^1\psi_{13}^1\psi_{21}^1\psi_{22}^1\psi_{23}^1\}$ and $\{w^1\}' = \{w_1^1 w_2^1 w_3^1\}$, such that,

$$[\boldsymbol{K}^1]\{\delta'\} = \begin{bmatrix} \boldsymbol{K}_{\psi\psi}^1 & \boldsymbol{K}_{\psi w}^1 \\ \boldsymbol{K}_{w\psi}^1 & \boldsymbol{K}_{ww}^1 \end{bmatrix} \begin{Bmatrix} \psi^1 \\ w^1 \end{Bmatrix}. \tag{20}$$

By putting eq. (19) into eqs (17) and (18), and making use of eqs (12)–(16), the stiffness matrix for element 2 is expressed as

$$[\boldsymbol{K}^2] = [\boldsymbol{S}]_0^1 + \frac{1}{\lambda}[\boldsymbol{S}]_1^1 + \frac{1}{\lambda^2}[\boldsymbol{S}]_2^1, \tag{21}$$

where

$$[\boldsymbol{S}]_0^1 = \begin{bmatrix} \boldsymbol{K}_{\psi\psi}^1 & 0 \\ 0 & 0 \end{bmatrix}, [\boldsymbol{S}]_1^1 = \begin{bmatrix} 0 & \boldsymbol{K}_{\psi w}^1 \\ \boldsymbol{K}_{w\psi}^1 & 0 \end{bmatrix} \text{ and } [\boldsymbol{S}]_2^1 = \begin{bmatrix} 0 & 0 \\ 0 & \boldsymbol{K}_{ww}^1 \end{bmatrix}. \tag{22}$$

Equation (21) can be used to calculate any DKT element with geometric similarity. A list of Fortran coding for the DKT element can be found in ref. [14].

FRACTAL TRANSFORMATION TECHNIQUE

The F2LFEM is based on the separation of the sub-domain $\boldsymbol{D}$ which contains the singularity from the complete cracked plate by an artificial surface boundary Γ (Fig. 2). Within $\boldsymbol{D}$ the solution is obtained by the F2LFEM on one hand, and outside $\boldsymbol{D}$ the solution is obtained by conventional FEM on the other hand. The generalized stiffness matrix in domain $\boldsymbol{D}$ is evaluated by transforming

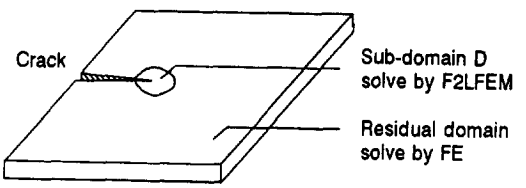

Fig. 2. Sub-domain D and residual domain.

the stiffness matrix of the first layer of mesh (Fig. 3) and modifying each element of the mentioned generalized stiffness matrix.

For the first layer of mesh, let the displacements on the boundary Γ be the masters $\{\delta_m\}$ and the displacements within the boundary Γ be the slaves $\{\delta_s\}$. To carry out the transformation, the stiffness matrix $[\boldsymbol{K}]$ in eq. (23) is first partitioned with respect to s and m,

$$[\boldsymbol{K}]\{\delta\} = \begin{bmatrix} \boldsymbol{K}^f_{ss} & \boldsymbol{K}^f_{sm} \\ \boldsymbol{K}^f_{ms} & \boldsymbol{K}^f_{mm} \end{bmatrix} \begin{Bmatrix} \delta_s \\ \delta_m \end{Bmatrix}, \tag{23}$$

where the superscript "f" indicates the first layer of mesh. The displacements at the slaves are transformed. The second level (global) interpolation of displacements can be written as follows,

$$\begin{Bmatrix} \delta_s \\ \delta_m \end{Bmatrix} = \begin{bmatrix} \boldsymbol{T}^f & 0 \\ 0 & \boldsymbol{I} \end{bmatrix} \begin{Bmatrix} \boldsymbol{a} \\ \delta_m \end{Bmatrix}, \tag{24}$$

where the transformation matrix $\boldsymbol{T}^f = \boldsymbol{T}^f_1 + \boldsymbol{T}^f_2$ can be evaluated by using eqs (7a), (7b) and (8) for $\boldsymbol{T}^f_1$ and eqs (7c) and (8) for $\boldsymbol{T}^f_2$; and $\boldsymbol{a}$ is the generalized coordinates vector. After transformation we have,

$$\begin{bmatrix} \boldsymbol{T}^{ft}\boldsymbol{K}^f_{ss}\boldsymbol{T}^f & \boldsymbol{T}^{ft}\boldsymbol{K}^f_{sm} \\ \boldsymbol{K}^f_{ms}\boldsymbol{T}^f & \boldsymbol{K}^f_{mm} \end{bmatrix} \begin{Bmatrix} \boldsymbol{a} \\ \delta_m \end{Bmatrix} = \begin{Bmatrix} 0 \\ 0 \end{Bmatrix}. \tag{25}$$

For the inner layer, each element stiffness matrix within the first layer of $\boldsymbol{D}$ would be transformed and assembled. Based on fractal concepts, an infinite number of elements and numerous number of degrees of freedom would be generated near the crack tip. Applying the fast transformation technique, infinitely many layers of mesh can be transformed and assembled.

Consider the matrix transformation of the k-th inner layer of the element stiffness matrix and the assembly of the inner layer of meshes form the 2-nd layer to the infinite layer, the generalized stiffness matrix is given as

$$\sum_{i=1}^{2}\sum_{j=1}^{2}\sum_{k=2}^{\infty} \boldsymbol{T}^{kt}_i \boldsymbol{K}^k \boldsymbol{T}^k_j = \sum_{i=1}^{2}\sum_{j=1}^{2}\sum_{l=0}^{2}\sum_{k=2}^{\infty} \boldsymbol{T}^{kt}_i \boldsymbol{S}^k_l \boldsymbol{T}^k_j \text{ and } \lambda = \frac{1}{2}. \tag{26}$$

In addition, because the matrices $\boldsymbol{T}^k_i$, $\boldsymbol{T}^k_j$ and $\boldsymbol{S}^k_l$ are not full, matrices multiplication of $\boldsymbol{T}^{kt}_i \boldsymbol{S}^k_l \boldsymbol{T}^k_j$ is non-zero only when

$$\begin{aligned} &i = j = 1 \text{ and } l = 0; \\ &i = j = 2 \text{ and } l = 2 \text{ or} \\ &i \neq j \text{ and } l = 1. \end{aligned} \tag{27}$$

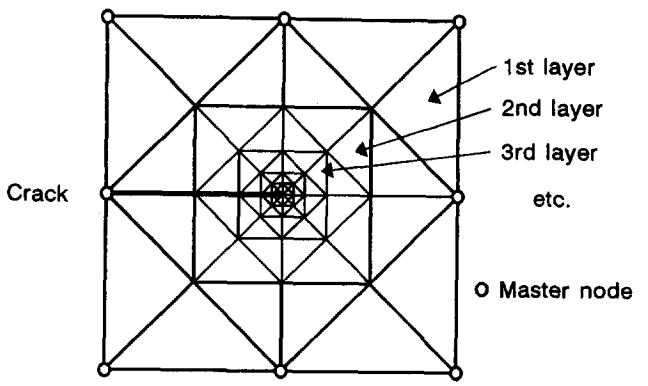

Fig. 3. Fractal mesh configuration. (Only the first layer of mesh is prepared, the rest will be generated automatically.)

With the fact of geometric similarity, (T^k_{1n}) the n-th term of the transformation matrix T^k_1 can be related to that of the first layer as,

$$T^k_{1n} = \lambda^{(k-1)(n-1)/2} T^f_1 . \tag{28}$$

Similarly,

$$T^k_{2n} = \lambda^{(k-1)(n+1)/2} T^f_2 . \tag{29}$$

Therefore, the sub-matrices ($\bar{K}^{kl}_{mn}$) of generalized stiffness matrix ($T^{kt}_i S^k_l T^k_j$) can be related to the first layer, such that
for $i = j = 1$ and $l = 0$

$$\bar{K}^{k0}_{mn} = T^{kt}_{1m} S^k_0 T^k_{1n} = [\lambda^{(m+n-2)/2}]^{k-1} \bar{K}^{f0}_{mn}$$

for $i \neq j$ and $l = 1$

$$\bar{K}^{k1}_{mn} = T^{kt}_{im} S^k_1 T^k_{jn} + T^{kt}_{jm} S^k_1 T^k_{in} = [\lambda^{(m+n-2)/2}]^{k-1} \bar{K}^{f1}_{mn}$$

for $i = j = 2$ and $l = 2$

$$\bar{K}^{k2}_{mn} = T^{kt}_{2m} S^k_2 T^k_{2n} = [\lambda^{(m+n-2)/2}]^{k-1} \bar{K}^{f2}_{mn} . \tag{30}$$

Hence, infinite series in eq. (26) can be replaced by the geometrical progression series and

$$\sum_{l=0}^{2} \sum_{k=2}^{\infty} \bar{K}^{kl}_{mn} = \frac{\epsilon}{1-\epsilon} \sum_{l=0}^{2} \bar{K}^{fl}_{mn} , \tag{31}$$

where $\epsilon = \lambda^{(m+n-2)/2}$. The result of eq. (31) suggests further simplification, as

$$\sum_{l=0}^{2} \bar{K}^{fl}_{mn} = T^{fl}_m K^f T^f_n , \tag{32}$$

where T^f_n is the n-th term of the transformation matrix T^f. Consequently, eq. (32) indicates that the generalized stiffness matrix for all the inner layers of the elements can be evaluated by simply transforming the first layer of the element stiffness matrix [eq. (20) instead of eq. (21)] and modifying each element in the first layer generalized stiffness matrix in turn by a factor shown in eq. (31). The complete generalized stiffness matrix can be calculated by making use of eqs (25), (31) and (32).

NUMERICAL EXAMPLE

The following examples are used to illustrate the effectiveness of the method. Discussion will be given on the results obtained by Kirchhoff's theory and from Reissner's plate theory. Consider a centre cracked square plate of edge length $2b$ and with crack length $2a$. The plate is subjected to edge moments as shown in Fig. 4. Because of symmetry, a quarter of the plate is used in the analysis, and it is divided into 220 triangular elements and 150 nodes. A typical mesh configuration

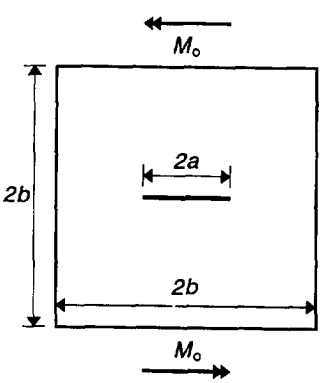

Fig. 4. Centre cracked plate subjected to edge moment.

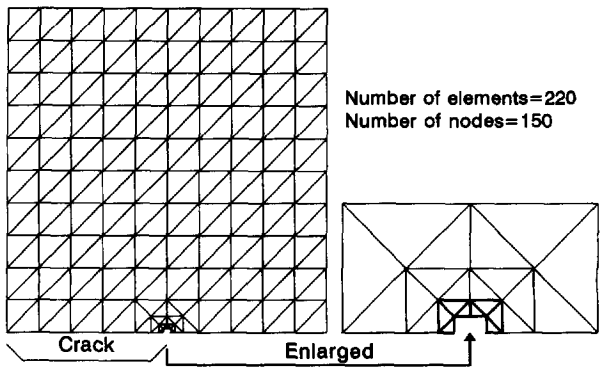

Fig. 5. A typical mesh configuration.

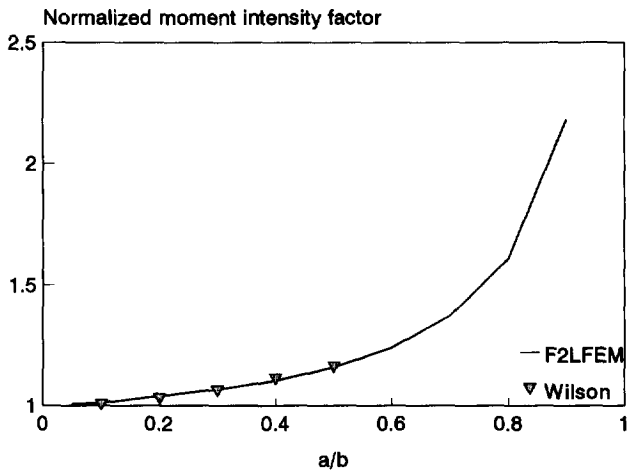

Fig. 6. Moment intensity factor for a square platae with central cracks subjected to edge moment.

for the ratio crack length per edge length ($a/b = 0.5$) is depicted in Fig. 5. Analytical results for an infinite plate with a centre crack are available [1].

$$K_1 = M_0\sqrt{a}\,. \tag{33}$$

By slightly modifying the sizes of mesh in Fig. 5, a mesh with ratio $a/b = 0.05$ is obtained. The convergency of the dimensionless moment intensity factor ($K_1/M_0\sqrt{a}$) against the number of transformation term is studied, the results are tabulated in Table 1. It is found that 14 transformation terms have attained a good convergence.

Figure 6 is a plot of the moment intensity factor for a square plate with central cracks subjected to edge moment. It is observed that in the range $0.1 \leq a/b \leq 0.5$ the results provided by F2LFEM follow almost exactly the data reported by Wilson and Thompson [5]. The present method seems

Table 1. Number of transformation terms against moment intensity factor, $a/b = 0.05$ (analytical solution for infinite plate with centre crack = 1.000)

Number of terms	2	4	6	8	10	12	14	16
$K_1/M_0\sqrt{a}$	0.973	0.985	0.998	1.001	1.006	1.006	1.007	1.007

Table 2. Comparison between the moment intensity factors determined by Kirchhoff's theory (present) and Reissner's theory [8] for cracked square plate. ($b/h = 10$, $v = 0.3$)

a/b	0.1	0.2	0.3	0.4	0.5	0.6	0.7	0.8	0.9
Kirchhoff's theory	0.320	0.465	0.584	0.698	0.819	0.961	1.147	1.438	2.065
Reissner's theory	0.238	0.322	0.394	0.465	0.544	0.641	0.774	0.996	1.534
Difference %	34.2	44.7	48.5	50.0	50.5	50.0	48.2	44.4	34.6

to be more efficient in terms of computation time, storage and more convenience in the sense of mesh preparation than the displacement extrapolation method as suggested by Wilson.

Finally, the results of moment intensity factors determined by Kirchhoff's theory are compared with those by Reissner's plate theory [8], as shown in Table 2. It is observed that for the same plate thickness of ratio $2b/h = 20$, Kirchoff's theory always gives an over-estimate of the moment intensity factor by up to 50%. The differences in the predictions of stress intensity factors between Kirchhoff's and Reissner's theory for cracked infinite plate had been discussed by Hartranft and Sih [3], and Wang [4] who obtained similar results as ours. Hartranft's results show that the difference can increase to 62% when the plate thickness increases from zero to approximately one-tenth of the crack length for $\nu = 0.3$.

CONCLUSIONS

The extension of the fractal two-level finite element method to a cracked plate by Kirchhoff's theory has been discussed. In the paper, the property of shape similarity of DKT element is discussed, fractal transformation technique is also introduced to transform the infinite number of nodal displacements vector around the crack tip to a new set of generalized displacements. The number of unknowns is reduced significantly and hence the computational effort is substantially decreased. The results are in good agreement with those obtained by the analytical method and displacement extrapolation method. Results of finite cracked plate are also compared with those obtained by Reissner's (shear deformation) theory; it is found that the predicted moment intensity factors by the two theories differ greatly up to about 50%. Finally, the present method can also be extended to apply for mixed mode crack problems or dynamic crack problems.

Acknowledgement—The research is supported by the Research Grant Council of Hong Kong.

REFERENCES

[1] G. C. Sih, P. C. Paris and F. Erdogan, Crack-tip, stress-intensity factors for plate extension and plate bending problems. *ASME, J. appl. Mech.* **29,** 306–312 (1962).
[2] J. K. Knowles and N. M. Wang, On the bending of an elastic plate containing a crack. *J. Math. Phys.* **39,** 223–236 (1960).
[3] R. J. Hartranft and G. C. Sih, Effect of plate thickness on the bending stress distribution around through cracks. *J. Math. Phys.* **47,** 276–281 (1968).
[4] N. M. Wang, Effect of plate thickness on the bending of an elastic plate containing a crack. *J. Math. Phys.* **47,** 371–389 (1968).
[5] W. K. Wilson and D. G. Thompson, On the finite element method for calculating stress intensity factors for cracked plates in bending. *Engng Fracture Mech.* **3,** 97–102 (1971).
[6] M. V. V. Murthy, K. N. Raja and S. Viswanath, On the bending stress distribution at the tip of a stationary crack from Reissner's theory. *Int. J. Fracture* **17,** 537–552 (1981).
[7] H. Boduroglu and F. Erdogan, Internal and edge cracks in a plate of finite width under bending. *ASME, J. appl. Mech.* **50,** 621–629 (1983).
[8] A. Y. T. Leung and R. K. L. Su, Fractal two-level finite element analysis of cracked Reissner's plate. *Thin Walled Structures* **24,** 315–334 (1996).
[9] A. Y. T. Leung and R. K. L. Su, Fractal two level finite element methods for 2-D crack problems. *Proc. 2nd Asian-Pacific Conf. on Computational Mech.* (pp. 675–679). A.A. Balkema/Rotterdam Brookfield (1993).
[10] A. Y. T. Leung and R. K. L. Su, Mode I crack problems by fractal two-level finite element method. *Engng Fracture Mech.* **48,** 847–859 (1994).
[11] M. L. Williams, The bending stress distribution at the base of a stationary crack. *ASME, J. appl. Mech.* **28,** 78–82 (1961).
[12] J. A. Stricklin, W. Haisler, P. Tisdale and R. A. Gunderson, A. Rapidly converging triangular plate element. *AIAA J.* **7,** 180–181 (1969).
[13] J. L. Batoz, K. J. Bathe and L. W. Ho, A study of three-node triangular plate bending elements. *Int. J. numer. Meth. Engng* **15,** 1771–1812 (1980).
[14] C. Jeyachandrabose and J. Kirkhope, An alternative explicit formulation for the DKT plate-bending element. *Int. J. numer. Meth. Engng* **21,** 1289–1293 (1985).

(*Received* 9 *December* 1994)